Received 30 August 2020; accepted 16 September 2020. Date of publication 21 September 2020; date of current version 9 October 2020.
The review of this article was arranged by Editor M. Chan.

Digital Object Identifier 10.1109/JEDS.2020.3025511

Modeling the Displacement Damage on Trigger Current of Anode-Short MOS-Controlled Thyristor

LEI LI [1,2] (Member, IEEE), ZE HONG LI [2] (Senior Member, IEEE), YU ZHOU WU [2], XIAO CHI CHEN [1], JIN PING ZHANG [2] (Member, IEEE), MIN REN [2] (Member, IEEE), YUAN JIAN [1], AND BO ZHANG [2] (Senior Member, IEEE)

1 Institute of Nuclear Physics and Chemistry, Chinese Academy of Engineering Physics, Mianyang 621000, China
2 State Key Laboratory of Electronic Thin Films and Integrated Devices, University of Electronic Science and Technology of China, Chengdu 610000, China

CORRESPONDING AUTHORS: L. LI AND Z. H. LI (e-mail: skyhappier@caep.cn; lizh@uestc.edu.cn)

ABSTRACT The MOS-controlled Thyristor (MCT) has been characterized by MOS-gating, high current rise rate, and high blocking capability. The anode short MCT (AS-MCT) is distinguished from conventional MCT by an anode-short structure, which develops a normally-off characteristic. As a composite structure made of metal-oxide-silicon and bipolar junction transistors, AS-MCT is susceptible to displacement damage induced by energetic radiation. The anode trigger current which denotes the latch-up of internal thyristor structure is a key parameter for AS-MCTs. From the aspects of devices physics, we propose a model to describe the displacement damage on trigger current. Our model provides an excellent fit to the experimental data of the AS-MCT samples subjected to fission neutrons with flux in the range of $3.1 \times 10^9 - 5.5 \times 10^{13}$ cm^{-2}. Moreover, this work shows that the high injection effect can alleviate the displacement damage of trigger current following high flux exposures.

INDEX TERMS Anode-short MOS-controlled thyristor, displacement damage, modeling, bipolar devices.

I. INTRODUCTION

Pulse discharge technology based on capacitive energy storage has been extensively used in several fields such as industrial area (extreme ultraviolet source), scientific research (nuclear fission driver) and so on [1]–[5]. Owing to the surge in current capability without current saturation, but with high current density up to 10^3 A $\cdot$ cm^{-2} and high current rising rate of $\sim 10^3 - 10^6$ A $\cdot$ μs^{-1}, as well as metal-oxide-silicon (MOS) gating, MOS-controlled Thyristor (MCT) is the natural switching unit for pulse discharge applications [3], [5]–[8]. A conventional MCT structure requires a gate voltage to form OFF-FET channel extracting carriers, and henceforth realizing a high blocking capability, which complicates the driver circuit and hampers the system reliability [7]. The anode-short MCT (AS-MCT), proposed over the last ten years [3], [8], features a normally-off characteristic owing to the introduction of an anode-short structure as presented in Fig. 1. The AS-MCT is a potential alternative to conventional MCT for pulse power applications.

In radiation environments, e.g., space mission, the MCTs suffer from the displacement damage (DD) induced by energetic radiation [9], such as neutrons and electrons. The DD sensitivity is intrinsic for silicon material, and refers to the dislodging of atoms from their normal lattice sites in a target material by impinging energetic radiation. The defect clusters in silicons can reduce minority carrier lifetime, change majority carrier density, and reduce carrier mobility [10]–[12]. Among these changes, the minority carrier lifetime is the most sensitive electronic property of silicon in the DD environment. The electron irradiation, ~MeV and $\sim 10^{11} - 10^{13}$ cm^{-2}, is a typical method for carrier lifetime control via the introduction of point-like defects, which results in an increase of the on-state voltage and a decrease of the turn-off time for MCTs [13], [14]. However,

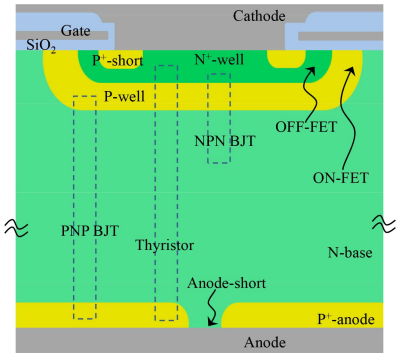

FIGURE 1. Cross section of cell unit for AS-MCT with N-type base region.

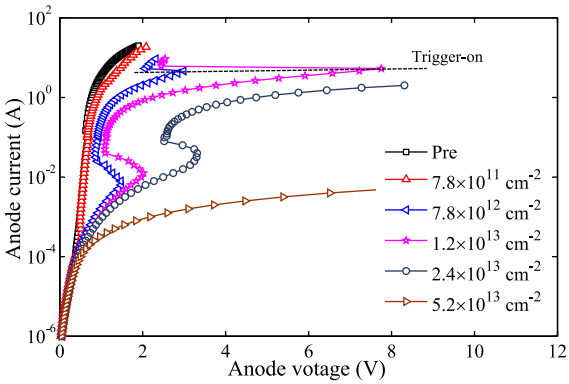

FIGURE 2. Forward anode current-voltage curves of AS-MCTs before and after neutron exposures. During measurements, the gate voltage is fixed at 5 V, which is larger than the threshold voltage (~0.5 V). This figure is a redrawing of [3, Fig. 7].

the study on DD effect for MCTs is apparently lagging in progress.

The previous works in 1989 [15] and 2017 [4] have reported the neutron-induced DD effects on conventional MCTs. Recently, our collaboration present the neutron induced DD effect on AS-MCTs [3], which indicates that the degradation of trigger current is fatal. Once the anode current exceeds a critical value, named by trigger current, the AS-MCT enters a thyristor-like mode which effectuates a conductive modulation effect in device and results in a small on-state resistance, ~mΩ. After middle flux neutron exposures, $\sim 10^{12}$ cm^{-2}, the trigger current can amplify by three orders of magnitude from mA to A as depicted in Fig. 2. For the cases of high flux neutron exposures, larger than $\sim 10^{13}$ cm^{-2}, the trigger current can surpass the capacity of power source. Thereafter, the AS-MCT can not be ignited, i.e., an functional failure occurs. Under such conditions, the conductive modulation effect do not exist in AS-MCTs, and the on-state resistance drastically increases to a large value of the order of 10 Ω. Then, an undesired power consumption occurs. The trigger current, a critical parameter, is suitable to characterize the DD tolerance of AS-MCTs. Unfortunately, this parameter is not modelled in the previous work [3].

From the prospective of device physics, this work presents the modeling for the trigger current of AS-MCTs. Moreover, we propose the mechanism for the degradation of the trigger current from DD in AS-MCTs. Owing to the essential physics of DD being the same in both N-base and P-base AS-MCT, we focus on the N-base AS-MCT for the sake of brevity. For the purpose of generality, we discuss the current density in device instead of terminal current during the modeling work.

TABLE 1. Symbols and parameters for AS-MCT.

Parameters	Value
P^+-anode/N-base junction (J_1)	–
P-well/N-base junction (J_2)	–
P-well/N^+-cathode junction (J_3)	–
Chip area (S)	0.48 cm^2
Total current density (J_A)	–
Trigger current density (J_{tr})	–
Electron current density of J_1 ($J_{1\text{-}e}$)	–
Hole current density of J_1 ($J_{1\text{-}h}$)	–
Electron current density of J_3 ($J_{3\text{-}e}$)	–
Hole current density of J_3 ($J_{3\text{-}h}$)	–
Recombination current density in P-well ($J_{3\text{-}r1}$)	–
Recombination current density in J_1 ($J_{3\text{-}r2}$)	–
Ideality factor of $J_{3\text{-}r2}$ (n)	–
Electron current density collected by the anode-short structure (J_{AS})	–
N-base sheet resistance ($\rho_\square$)	–
Length of P^+-anode in half cell (L_{AS})	9.0 μm
Length of half cell (L)	10.0 μm
Anode contact resistance (R_A)	45.0 Ω·m^{-2}
Hole diffusion length (L_p)	–
Electron diffusion length (L_n)	–
Ambipolar diffusion length (L_a)	–
Carriers lifetime (τ)	–
Ambipolar lifetime (τ_a)	–
Initial value of τ (τ_0)	400.0 μs
Hole diffusion coefficient (D_p)	15.0 cm^2·s^{-1}
Electron diffusion coefficient (D_n)	30.0 cm^2·s^{-1}
Ambipolar diffusion coefficient (D_a)	10.0 cm^2·s^{-1}
P^+-anode width ($W_{P\text{-anode}}$)	2.0 μm
N-base width ($W_{N\text{-base}}$)	600.0 μm
P-well width ($W_{P\text{-well}}$)	10.0 μm
N^+-cathode width ($W_{N\text{-cathode}}$)	2.0 μm
Depletion region width of J_3 (W_{J3})	0.5 μm
P^+-anode doping concentration ($N_{P\text{-anode}}$)	1.0×10^{18} cm^{-3}
P^+-anode doping concentration ($N_{N\text{-base}}$)	1.6×10^{13} cm^{-3}
P^+-anode doping concentration ($N_{P\text{-well}}$)	5.0×10^{15} cm^{-3}
N^+-cathode doping concentration ($N_{N\text{-cathode}}$)	5.0×10^{17} cm^{-3}

II. MODELING THE DD FOR AS-MCT TRIGGER CURRENT

A. TRIGGER-ON OF AS-MCT

An AS-MCT is comprised of thousands of cells, and each cell is a composite structure of MOS transistors and Bipolar-Junction-Transistors (BJT) as shown in Fig. 1. The N-base and P-well serve as the common regions for the upper N^+-well/P-well/N-base (NPN) and lower P-well/N-base/P^+-anode (PNP) BJTs. The trigger-on of AS-MCT denotes the latch-up of vertical N^+-well/P-well/N-base/P^+-anode (PNPN) thyristor structure, i.e., the coupling of the two BJTs. Its criterion can be expressed as [3], [16]

$$\alpha_{PNP} + \alpha_{NPN} \geq 1 \tag{1}$$

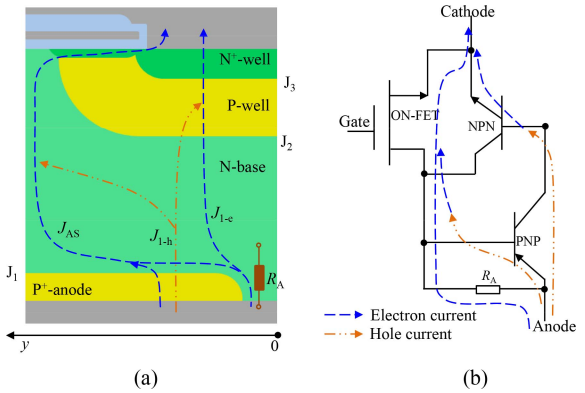

FIGURE 3. Current flow lines (a) and equivalent circuits (b) for an un-trigged AS-MCT. In (a), only the half-cell is plotted. The OFF-FET structure is omitted.

where α_{PNP} and α_{NPN} are the open-base (or common-base) current gains of PNP and NPN respectively. The AS-MCT features a normally-off characteristic (gate anode is zero biased) owing to the introduction of anode-short structure. The emitter-base junction of PNP is also shorted by such a structure, and then, α_{PNP} is suppressed which is nearly zero for the case of small anode current. Under such conditions, the AS-MCTs are operated in blocking mode, and the upper NPN with wide collector region (N-base) is capable of supporting the high voltage. Table 1 lists the symbols and parameters for AS-MCTs.

Fig. 3 illustrates the current flow lines in AS-MCTs. When a positive gate bias is applied, the ON-FET is gradually turned on, and the electrons flow from the N^+-well into the N-base region. Then these electrons flow through the N-base region. These electrons are by-passed and collected by the anode-short structure. The electron current will induce a voltage drop across the P^+-anode/N-base junction (J_1), which results in the hole injection from P^+-anode into N-base. Part of holes recombine with electron in N-base, which serves as the base drive current for lower PNP. The survival holes passing through the N-base region are collected by the P-well/N-base junction (J_2), and serve as the base drive current for upper NPN. Both α_{PNP} and α_{NPN} in (1) are proportional to their own base currents. The minimum anode current which makes (1) satisfied is referred to the trigger current. The trigger current density (J_{tr}) can be calculated by

$$\alpha_{PNP}(J_{tr}) + \alpha_{NPN}(J_{tr}) = 1 \tag{2}$$

In the following Sections II-B to II-C, we derive the formulas for α_{NPN} and α_{PNP} respectively. And in Section II-D, we model the DD damage in AS-MCTs.

B. CURRENT GAIN OF LOWER PNP

The lower PNP structure in AS-MCT is characterized by a emitter-base short structure and a wide base. Analogy to the conventional PNP, α_{PNP} of lower PNP can be expressed as

$$\alpha_{PNP} = \gamma_{PNP}\beta_{PNP} \tag{3}$$

where γ_{PNP} and β_{PNP} are emitter injection efficiency and base transport factor of PNP respectively. γ_{PNP} can be calculated by

$$\gamma_{PNP} = \frac{J_{1-h}}{J_A} \tag{4}$$

As presented in Fig. 3 (a), the total current density (J_A) near the anode electrode is the sum of three components [16], i.e.,

$$J_A = J_{1-e} + J_{1-h} + J_{AS} \tag{5}$$

The electron current (J_{AS}) horizontally flows across the N-base, and induces a voltage drop (V_{J1}) on J_1. V_{J1} can be calculated by the integral of voltage drop along J_1, i.e.,

$$V_{J1} = \int_0^L J_{AS}\rho_{\square}dy + J_{AS}R_A = \frac{1}{2}J_{AS}\rho_{\square}L_{AS}^2 + J_{AS}R_A \tag{6}$$

The latter part of (6) on the right-hand side is the voltage drop produced by the anode contact resistance (R_A). From the junction law for the forward-biased J_1, we know that

$$J_{1-e} = \frac{qD_n n_i^2}{W_{P-anode}N_{P-anode}}\exp\left(\frac{V_{J1}}{V_T}\right) \tag{7}$$

$$J_{1-h} = \frac{qD_p n_i^2}{L_a N_{N-base}}\exp\left(\frac{V_{J1}}{V_T}\right) \tag{8}$$

where q is the electron charge, n_i is the intrinsic carrier concentration and V_T is the thermal voltage.

β_{PNP} is a measure of the ability for the holes injected at J_1 to reach the J_2 junction. Part of the holes injected into the N-base are unable to reach the J_2 junction due to their recombination with electrons in the N-base. β_{PNP} is always less than unity for a BJT, and takes the form as

$$\beta_{PNP} = \cosh^{-1}\left(\frac{W_{N\text{-base}}}{L_a}\right) \tag{9}$$

The N-base (base of PNP) is slightly doped to avoid its punch-through for AS-MCT operated in the forward blocking mode. A high injection level can occur in the N-base at a relative small anode current, ~mA. Thereafter, we adopt the ambipolar diffusion coefficient (D_a) and ambipolar diffusion length (L_a) in (8) and (9) respectively, to account for the high-injection-induced decrease in β_{PNP} via carrier-carrier scattering phenomenon [16].

From (4)-(9), α_{PNP} in (3) can be rewritten as

$$\alpha_{PNP} = \cosh^{-1}\left(\frac{W_{N-base}}{L_a}\right)\left(\frac{qD_p n_i^2}{L_a N_{N-base}}\right) \times \left[\frac{qD_p n_i^2}{L_a N_{N-base}} + \frac{qD_n n_i^2}{W_{P-anode}N_{P-anode}} + J_{AS}\exp\left(\frac{-J_{AS}\rho_{\square}L_{AS}^2}{2V_T}\right)\right]^{-1}. \tag{10}$$

C. CURRENT GAIN OF UPPER NPN

α_{NPN} can be calculated by

$$\alpha_{\mathrm{NPN}} = \gamma_{\mathrm{NPN}}\beta_{\mathrm{NPN}} \tag{11}$$

where γ_{NPN} and β_{NPN} are emitter injection efficiency and base transport factor of upper NPN respectively. γ_{NPN} and β_{NPN} can be expressed as [9]

$$\gamma_{\mathrm{NPN}} = \frac{J_{3-\mathrm{e}}}{J_{3-\mathrm{e}} + J_{3-\mathrm{h}} + J_{3-\mathrm{r2}}} \tag{12}$$

$$\beta_{\mathrm{NPN}} = \cosh^{-1}\left(\frac{W_{\text{P-well}}}{L_{\mathrm{n}}}\right) \tag{13}$$

From the junction law for forward-biased J_3 junction, we know that $J_{3\text{-e}}$, $J_{3\text{-h}}$ and $J_{3\text{-r2}}$ can be expressed as

$$J_{3\text{-e}} = \frac{qD_{\mathrm{n}}n_{\mathrm{i}}^2}{L_{\mathrm{n}}N_{\text{P-well}}}\exp\left(\frac{V_{\mathrm{J3}}}{V_{\mathrm{T}}}\right) \tag{14}$$

$$J_{3\text{-h}} = \frac{qD_{\mathrm{p}}n_{\mathrm{i}}^2}{W_{\text{N-cathode}}N_{\text{N-cathode}}}\exp\left(\frac{V_{\mathrm{J3}}}{V_{\mathrm{T}}}\right) \tag{15}$$

$$J_{3\text{-r2}} = \frac{qW_{\mathrm{J3}}n_{\mathrm{i}}}{2\tau}\exp\left(\frac{V_{\mathrm{J3}}}{nV_{\mathrm{T}}}\right) \tag{16}$$

The voltage drop on J_3 (V_{J3}) can be figured out from the aspect of hole current density ($J_{\text{h-NPN}}$) in NPN. $J_{\text{h-NPN}}$ contains three components, including the back injection component in emitter ($J_{3\text{-h}}$), the recombination component in P-well ($J_{3\text{-r1}}$) and the recombination component in J_3 junction region ($J_{3\text{-r2}}$). $J_{3\text{-r1}}$ can be expressed as

$$J_{3\text{-r1}} = \frac{qW_{\text{P-well}}D_{\mathrm{n}}n_{\mathrm{i}}^2}{\tau N_{\text{P-well}}}\exp\left(\frac{V_{\mathrm{J3}}}{V_{\mathrm{T}}}\right) \tag{17}$$

As stated in Section II-A, the holes collected by J_2 servers as the hole current for NPN. Then, we know that

$$J_{3\text{-r1}} + J_{3\text{-r2}} + J_{3\text{-h}} = J_{1\text{-h}}\beta_{\mathrm{PNP}} \tag{18}$$

From (8) and (15)–(18), we can figure out V_{J3} via numerical calculation. Thereafter, from (12)-(16), α_{NPN} in (11) can be rewritten as

$$\alpha_{\mathrm{NPN}} = \cosh^{-1}\left(\frac{W_{\text{P-well}}}{L_{\mathrm{n}}}\right)\left(\frac{D_{\mathrm{n}}}{L_{\mathrm{n}}N_{\text{P-well}}}\right) \times \left\{\frac{D_{\mathrm{n}}}{L_{\mathrm{n}}N_{\text{P-well}}} + \frac{D_{\mathrm{p}}}{W_{\text{N-cathode}}N_{\text{N-cathode}}} + \frac{W_{\mathrm{J3}}}{2\tau n_{\mathrm{i}}}\exp\left[\frac{(1-n)V_{\mathrm{J3}}}{nV_{\mathrm{T}}}\right]\right\}^{-1} \tag{19}$$

In (19), V_{J3} is a function of J_{AS} and β_{PNP}. As the P-well is heavily doped, the carrier injection level in P-well is small. Thereafter, the electron diffusion length (L_{n}) and coefficient (D_{n}) are adopted to calculate α_{NPN}.

D. DD DAMAGE

After DD, the degradation of minority carrier lifetime dominates the degradation of α_{PNP} and α_{NPN} [3], [9]–[12]. The change of the reciprocal of the minority carrier lifetime increases linearly with the increase of the particle flux (Φ) [9], i.e.,

$$\frac{1}{\tau} - \frac{1}{\tau_0} = K\Phi \tag{20}$$

where K is the damage factor, typically in the range of 10^{-18}-10^{-16} $\mathrm{cm^2{\cdot}s^{-1}}$. For AS-MCT, K can be extracted from the leakage current readings [9]. In this work, Φ is the 1 MeV neutron equivalent flux.

The electron diffusion length (L_{n}) and ambipolar diffusion length (L_{a}) in (10) and (19) are determined by the carrier lifetime, which can be calculated by

$$L_{\mathrm{n}} = \sqrt{D_{\mathrm{n}}\tau} = \sqrt{\frac{D_{\mathrm{n}}}{K\Phi + 1/\tau_0}} \tag{21}$$

$$L_{\mathrm{a}} = \sqrt{D_{\mathrm{a}}\tau_{\mathrm{a}}} = \sqrt{\frac{2D_{\mathrm{a}}}{K\Phi + 1/\tau_0}} \tag{22}$$

The ambipolar lifetime (τ_{a}) in (22) can be calculated by

$$\tau_{\mathrm{a}} = \frac{\tau_{\mathrm{p}}\tau_{\mathrm{n}}}{\tau_{\mathrm{p}} + \tau_{\mathrm{n}}} \tag{23}$$

where τ_{p} are τ_{n} lifetimes of holes and electrons respectively. For simplification, we adopt that $\tau_{\mathrm{p}} = \tau_{\mathrm{n}} = \tau$ in this work. Equations (20)-(22) indicate that L_{n} and L_{a} decrease with increasing Φ, which result in the degradation of trigger current density (J_{tr}) after DD.

J_{tr} is designed on the order of $\sim\mathrm{mA{\cdot}cm^{-2}}$ to shorten the turn-on delay of AS-MCTs, ~100 ns. After DD, as presented in Fig. 2, J_{tr} increases significantly, and can reach up to $\sim\mathrm{A{\cdot}cm^{-2}}$ which corresponds to a high injection level in N-base region. Under such conditions, the carrier lifetime (τ) exhibits dependence on the carrier injection level, as both the hole (τ_{p}) and electron (τ_{n}) lifetimes in (23) depend on their respective quasi-fermi levels. For simplification, during the derivation of (20), the assumption of 1-level defect is adopted. Thus, K denotes the average damage effect induced by the real DD defect of multi energy levels. The effective lifetime (τ_{E}) can be expressed as

$$\tau_{\mathrm{E}} = \tau\left\{\left[1 + \frac{1}{1+h}\exp\left(\frac{E_{\mathrm{r}} - E_{\mathrm{F}}}{V_{\mathrm{T}}}\right)\right] + \zeta\left[\frac{h}{1+h} + \frac{1}{1+h}\exp\left(\frac{2E_{\mathrm{i}} - E_{\mathrm{r}} - E_{\mathrm{F}}}{V_{\mathrm{T}}}\right)\right]\right\} \tag{24}$$

where h is the normalized injection level of minority carrier, E_{F} is the fermi level of N-base in equilibrium, E_{i} is the intrinsic energy level, τ_{s} is the minority carrier lifetime in heavily doped silicon, and ζ is the ratio of the minority carrier lifetime in heavily doped P-type to that in heavily doped N-type silicon. In this work, $\zeta = 100$, $E_{\mathrm{r}} = E_{\mathrm{i}} = 0.55$ eV and $E_{\mathrm{F}} = 0.73$ eV. Fig. 4 presents the dependence of normalized lifetime ($= \tau_{\mathrm{E}}/\tau$) on the injection level (h). For N-base, h can be calculated by

$$h = \frac{p}{p_0} - 1 = \frac{rJ_{1\mathrm{h}}\tau_{\mathrm{s}}N_{\text{N-base}}}{qW_{\text{N-base}}n_{\mathrm{i}}^2} - 1 \tag{25}$$

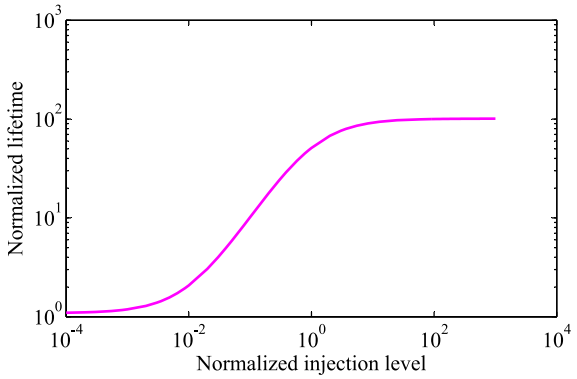

FIGURE 4. Dependence of hole lifetime on injection level. The results are calculated by (25).

where p_0 is the equilibrium concentration of holes, p is the concentration of holes, and r is a modifier factor which accounts for the average value of p in the thick N-base. r is $\sim 10^{-10}$ in this work.

III. EXPERIMENTAL VALIDATION

A. SAMPLES AND EXPERIMENTS

The AS-MCTs examined here are fabricated with the commercial insulated gate bipolar translator (IGBT) process [3], [5]. Fig. 5 presents the structure of AS-MCT chip. The fabricated devices show a forward blocking capability of ~1800 V at the gate-ground and a static forward voltage drop of 1.5 V at an anode current of 12 A. Table 1 lists the key parameters of our samples. The devices from single diffusion lots were irradiated by CFBR-II fast neutron reactor [3]. The CFBR-II is a "dry-type" reactor, and its reactor core is mounted in a shielding room [17]. The samples are placed outside the core, and both the core and samples are in air atmosphere. Thus, during experiment, the temperatures of samples are almost unchanged. The reactor was operated in the steady-state mode, and the average neutron energy is ~1.2 MeV.

Nine groups of samples were placed at different locations with different distances from the reactor core, and the samples were irradiated with series of neutron flux, which ranges from 3.1×10^{9} to 5.5×10^{13} cm^{-2}. Each group contains three devices. The neutron fluxes on samples were measured with (^{32}S) foil activation method. The uncertainties on the neutron flux is about ±9%. Both irradiations and measurements have been performed at room temperatures. The electrical parameters of AS-MCTs were measured by Keithley 2636B-PCT power device curve tracer. In the following Section III-B, the average value of the three measured data from devices in a group is presented. For devices in a group, the deviation of data ranges from ±15% to ±50%. For conservation and simplification, we adopt the maximum deviation for all groups when plotting the error bars.

As stated in Section II-D, the lifetime damage factor (K) in (20) can be extracted from the leakage current readings of AS-MCTs [9]. For our samples, K is about

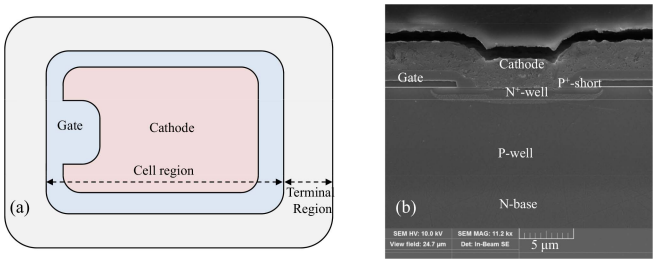

FIGURE 5. The features of XND1 AS-MCT. (a)-Illustration of the layer out of chip, and (b)-Scanning electron microscopy image of vertical appearance of cell unit. In (a), the cell region is with the size of 10.0 mm×6.4 mm. The cell unit is with the size of 20 μm (Width) ×625 μm (Thickness), and (b) presents the top region of a cell. A chip contains 1.3×10^{5} cell units.

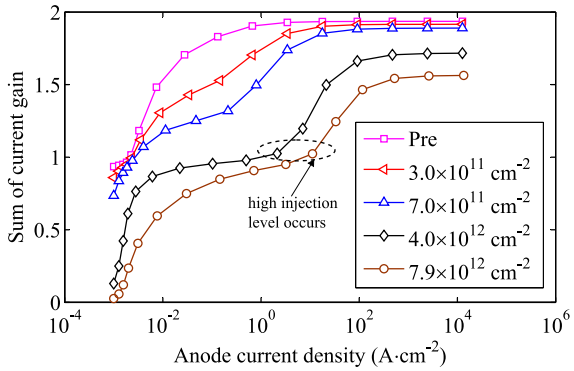

FIGURE 6. The dependence of total current gain on anode current density of AS-MCT before and after neutron irradiation. The results are calculated by our model.

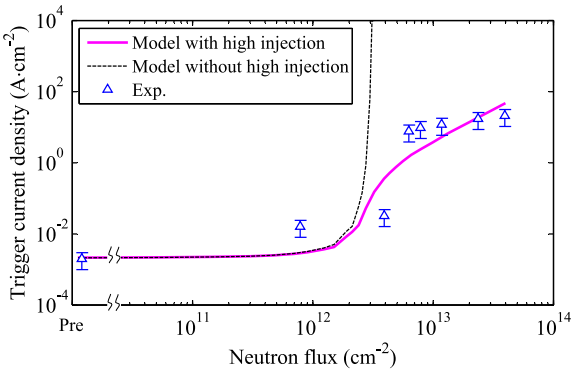

FIGURE 7. The dependence of trigger current density of AS-MCT on neutron flux. The experimental results are extracted from the data in Fig. 2.

2.5×10^{-8} cm$^2\cdot$s^{-1}. A TCAD simulation shows that the initial lifetime (τ_0) of 400 μs provides a good fit for the leakage current readings of our samples. Thus, in the following calculation, we take $\tau_0 = 400$ μs.

B. DD OF TRIGGER CURRENT

From (10), (19) and (21)–(25), we can figure out the dependence of total current gain ($\alpha_{PNP}+\alpha_{NPN}$) on anode current density before and after DD, as presented in Fig. 6. Thereafter, the trigger current density (J_{tr}) can be extracted under the constraint described in (2), i.e., $\alpha_{PNP}+\alpha_{NPN}=1$. Fig. 7 shows the Φ dependence of J_{tr}. Overlaid on these

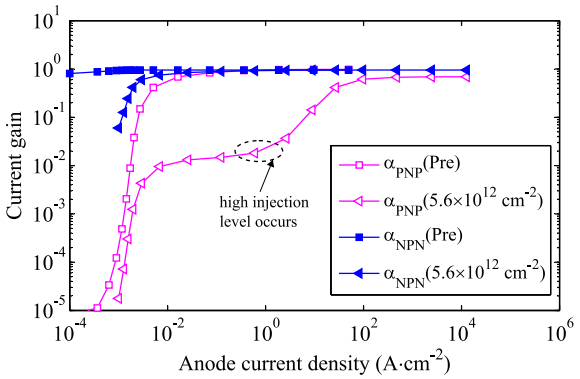

FIGURE 8. Change of the common-base current gain versus anode current density for AS-MCT before and after neutron exposures. α_{PNP} and α_{NPN} are calculated by (10) and (19) respectively.

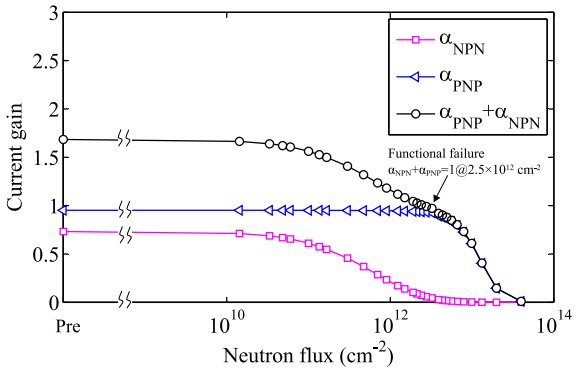

FIGURE 9. Change of the common-base current gain versus the neutron flux for AS-MCT. The common-base current gain of PNP structure (α_{PNP}) and that of NPN (α_{NPN}) are calculated by (10) and (19) respectively. During calculation, the anode current density is fixed at 100 mA·cm^{-2}.

data in Fig. 7 is the excellent agreement between the experimental data and model. The DD of J_{tr} exhibits dependence on neutron flux.

Subsequent to low Φ exposures, $\sim 10^{12}$ cm^{-2}, J_{tr} is almost unchanged and keeps on the order of $\sim$mA·cm^{-2}. For the case of middle Φ, up to $\sim 1.0\times10^{12}-4.0\times10^{12}$ cm^{-2}, J_{tr} increases significantly with increasing Φ. J_{tr} amplifies by several orders of magnitude, and reaches up to $\sim$A·cm^{-2}. For the case of high Φ, larger than 4.0×10^{12} cm^{-2}, the damage slope of J_{tr} decreases. The high injection mechanism is responsible for the alleviation effect of J_{tr} damage. As stated in Section II-D, the carrier lifetime is a function of carrier injection level. After high neutron flux exposures, the AS-MCT can be turned on by a large trigger current, which leads to a high injection level in N-base. Thereafter, the damage of hole lifetime in N-base can be depressed by such high injection effect. Then, α_{PNP} exhibits a further increase at higher anode current density ($\sim$10 A·cm^{-2}) as presented in Fig. 6. Thus, the high injection modulation effect alleviates the damage of J_{tr}. If we omit the high injection phenomenon, we will overestimate the DD damage of J_{tr} as illustrated in Fig. 7.

The trigger-on of AS-MCTs after very high Φ exposures will occur under the conditions of high anode voltage and current density, which exceed the capacity of power supply of test instrument. Then, we can not observe the trigger-on of AS-MCTs following very high Φ exposures, e.g., 5×10^{13} cm^{-2} for our samples as presented in Fig. 2.

IV. DISCUSSIONS

α_{NPN} and α_{PNP} are critical factors for the regenerative action of AS-MCTs. It is highly significant to understand the behaviours of α_{PNP} and α_{PNP}. Fig. 8 and 9 illustrate the dependence of such two parameters on anode current density (J_A) and Φ respectively. In this section, the behaviours of α_{PNP} and α_{NPN} are analyzed from the aspects of emitter injection efficiencies (γ_{PNP} and γ_{NPN}) and base transport factors (β_{PNP} and β_{NPN}).

For an un-irradiated AS-MCT, α_{NPN} is weakly dependent on J_A, and is larger than 0.85 even for the cases of small J_A, ≤ 100 μA·cm^{-2} as presented in Fig. 8. Whereas, α_{PNP} is very sensitive to J_A. Due to the introduction of anode-short structure, γ_{PNP} is depressed greatly which leads to that α_{PNP} approaches zero for a small J_A. γ_{PNP}, and thus α_{PNP}, increases drastically with increasing J_A. Once $J_A = J_{tr}$, the AS-MCT is turned on. After DD, the damage of minority carrier lifetime results in a degradation of carrier diffusion length (L_a and L_n, see Section II-D). Equations (9) and (13) indicate that the base transport factors are proportional to the carrier diffusion length. As the base width of the lower PNP ($\sim$600 μm) is much larger than that of the upper NPN ($\sim$10 μm), α_{PNP} (or β_{PNP}) is more sensitive to DD than α_{NPN} (or β_{NPN}), as presented in Fig. 8 and 9. For the cases of high Φ exposures, $\sim 10^{12}$ cm^{-2}, the lifetime decreases from hundreds of μs to several μs. The corresponding diffusion length decreases from $\sim$1000 μm to $\sim$100 μm. Thereafter, α_{PNP} (or β_{PNP}) is damaged significantly, which is about 10% of its initial value. As presented in Fig. 8, the high injection effect (see Section II-D) can alleviate the damage of α_{PNP} by depressing the DD-defect-related carrier recombination. Thus, the AS-MCTs can be turned on by a large J_{tr} with the order of A·cm^{-2} after high neutron flux exposures.

A smaller J_{tr} is preferred to a small power consumption and a shorter trigger-on delay-time for AS-MCTs. For a special application, a critical value of J_{tr} ($J_{tr\text{-}cri}$) can be defined to evaluate the effectiveness of AS-MCTs, e.g., 100 mA·cm^{-2} in Fig. 9. Thereafter, under the condition of $J_A = J_{tr\text{-}cri}$, we can quantitatively characterize the DD tolerance of AS-MCTs by a functional failure flux (Φ_F). A larger Φ_F means a better DD tolerance of AS-MCTs. The techniques, which can alleviate the decrease in α_{NPN} and α_{PNP}, can improve the Φ_F.

V. CONCLUSION

A general degradation model is proposed to describe the trigger current degradation of AS-MCTs induced by displacement damage. After displacement damage, the degradation of carrier lifetime dominates the increase of trigger current. The dependence of trigger current density (J_{tr}) on

particle flux (Φ) exhibits a "S-type" shape. J_{tr} is almost unchanged following low Φ exposures, and keeps on the order of mA·cm^{-2}. For the cases of middle Φ exposures, J_{tr} increases drastically with increasing Φ, which amplifies by several orders of magnitude, up to A·cm^{-2}. After high Φ exposures, the high carrier injection level exits in the N-base which can alleviate the damage of carrier lifetime in such region by depressing the DD-defect-related recombination. Under such conditions, the degradation of J_{tr} is alleviated, and the AS-MCTs can be triggered by a large J_{tr}, several A·cm^{-2}.

REFERENCES

[1] H. Akiyama, T. Sakugawa, T. Namihira, K. Takaki, Y. Minamitani, and N. Shimomura, "Industrial applications of pulsed power technology," *IEEE Trans. Dielectr. Electr. Insul.*, vol. 14, no. 5, pp. 1051–1064, Oct. 2007.

[2] T. Yokoo, K. Saiki, K. Hotta, and W. Jiang, "Repetitive pulsed high-voltage generator using semiconductor opening switch for atmospheric discharge," *IEEE Plasma Sci.*, vol. 36, no. 5, pp. 2638–2643, Oct. 2008.

[3] L. Li *et al.*, "Experimental study on displacement damage effects of anode-short MOS-controlled thyristor," *IEEE Trans. Nucl. Sci.*, vol. 67, no. 3, pp. 508–517, Apr. 2020, doi: 10.1109/TNS.2020.2971646.

[4] L. Li, Z. H. Li, M. Ren, J. P. Zhang, W. Gao, and Y. C. Lin, "Fast neutron irradiation effects of Silicon MOS-Controlled thyristor," in *Proc. IEEE 24th Int. Symp. Phys. Failure Anal. Integr. Circuits (IPFA)*, Chengdu, China, Jul. 2017, pp. 1–4.

[5] W. J. Chen *et al.*, "Design and characterization of high di/dt CS-MCT for pulse power applications," *IEEE Trans. Electron Devices*, vol. 64, no. 10, pp. 4206–4212, Oct. 2017.

[6] W. J. Chen *et al.*, "High peak current MOS gate-triggered thyristor with fast turn-on characteristics for solid-state closing switch applications," *IEEE Electron Device Lett.*, vol. 37, no. 2, pp. 205–208, Feb. 2016.

[7] F. Bauer, H. Hollenbeck, T. Stockmeier, and W. Fichtner, "Current-handling and switching performance of MOS-controlled thyristor (MCT) structures," *IEEE Electron Device Lett.*, vol. 12, no. 6, pp. 297–299, Jun. 1991.

[8] E. V. Chernyavskii, V. P. Popov, Y. S. Pakhmutov, and L. N. Safronov, "MOS-controlled thyristor: A study of a promising power-switching device," *Russ. Microelectron.*, vol. 31, no. 5, pp. 318–322, 2002.

[9] L. Li *et al.*, "Current gain degradation model of displacement damage for drift BJTs," *IEEE Trans. Nucl. Sci.*, vol. 66, no. 4, pp. 716–723, Apr. 2019.

[10] G. C. Messenger, "A summary review of displacement damage from high energy radiation in silicon semiconductors and semiconductor devices," *IEEE Trans. Nucl. Sci.*, vol. 39, no. 3, pp. 468–473, Jun. 1992.

[11] J. R. Srour, C. J. Marshall, and P. W. Marshall, "Review of displacement damage effects in silicon devices," *IEEE Trans. Nucl. Sci.*, vol. 50, no. 3, pp. 653–670, Jun. 2003.

[12] J. R. Srour and J. W. Palko, "Displacement damage effects in irradiated semiconductor devices," *IEEE Trans. Nucl. Sci.*, vol. 60, no. 3, pp. 1740–1766, Jun. 2013.

[13] E. V. Chernyavsky, V. P. Popov, Y. I. Krasnikov, and L. N. Safronov, "Carrier lifetime and turn-off current control by electron irradiation of MCT," *Nucl. Instrum. Methods Phys. Res. B, Interactions Mater. Atoms*, vol. 186, nos. 1–4, pp. 157–160, 2002.

[14] E. V. Chernyavsky, V. P. Popov, Y. S. Pakhmutov, Y. S. Krasnikov, and L. N. Safronov, "Dynamic and static characteristics of MOS thyristors irradiated with electrons," *Chem. Sustain. Develop.*, vol. 9, pp. 65–69, Mar. 2001.

[15] D. H. Loescher, W. R. Dawes, and D. B. King, "Co-60 and neutron irradiation of MOS-controlled thyristors," *IEEE Trans. Nucl. Sci.*, vol. 36, no. 6, pp. 2411–2414, Dec. 1989.

[16] B. J. Baliga, *Advanced High Voltage Power Device Concepts*. New York, NY, USA: Springer, 2011, pp. 398–436.

[17] X. B. Liu *et al.*, "Experimental study of neutron initiation probability at CFBR-II with pulsed neutrons," *Nucl. Sci. Eng.*, vol. 181, pp. 96–104, Sep. 2015.